Monthly Notices of the ROYAL ASTRONOMICAL SOCIETY

MNRAS **447,** 1761–1773 (2015) doi:10.1093/mnras/stu2546

The effect of massive neutrinos on the Sunyaev–Zel'dovich and X-ray observables of galaxy clusters

M. Roncarelli,[1,2]★ C. Carbone[3,4] and L. Moscardini[1,2,4]

[1] *Dipartimento di Fisica e Astronomia, Università di Bologna, viale Berti Pichat 6/2, I-40127 Bologna, Italy*
[2] *Istituto Nazionale di Astrofisica (INAF) – Osservatorio Astronomico di Bologna, via Ranzani 1, I-40127 Bologna, Italy*
[3] *Istituto Nazionale di Astrofisica (INAF) – Osservatorio Astronomico di Brera, via Bianchi 46, I-23807 Merate (LC), Italy*
[4] *Istituto Nazionale di Fisica Nucleare (INFN) – Sezione di Bologna, viale Berti Pichat 6/2, I-40127 Bologna, Italy*

Accepted 2014 December 1. Received 2014 November 5; in original form 2014 September 12

ABSTRACT

Massive neutrinos are expected to influence the formation of the large-scale structure of the Universe, depending on the value of their total mass, $\Sigma\, m_\nu$. In particular *Planck* data indicate that a non-zero $\Sigma\, m_\nu$ may help to reconcile cosmic microwave background data with Sunyaev–Zel'dovich (SZ) cluster surveys. In order to study the impact of neutrinos on the SZ and X-ray cluster properties we run a set of six very large cosmological simulations ($8\,h^{-3}$ Gpc^3 comoving volume) that include a massive neutrino particle component: we consider the values of $\Sigma\, m_\nu = (0,\ 0.17,\ 0.34)$ eV in two cosmological scenarios to test possible degeneracies. Using the halo catalogues extracted from their outputs we produce 50 mock light cones and, assuming suitable scaling relations, we determine how massive neutrinos affect SZ and X-ray cluster counts, the y-parameter and its power spectrum. We provide forecasts for the South Pole Telescope (SPT) and *extended Roentgen Survey with an Imaging Telescope Array* cluster surveys, showing that the number of expected detections is reduced by 40 per cent when assuming $\Sigma\, m_\nu = 0.34$ eV with respect to a model with massless neutrinos. However the degeneracy with σ_8 and Ω_m is strong, in particular for X-ray data, requiring the use of additional probes to break it. The y-parameter properties are also highly influenced by the neutrino mass fraction, f_ν, with $\langle y \rangle \propto (1 - f_\nu)^{20}$, considering the cluster component only, and the normalization of the SZ power spectrum is proportional to $(1 - f_\nu)^{25\text{–}30}$. Comparing our findings with SPT and Atacama Cosmology Telescope measurements at $\ell = 3000$ indicates that, when *Planck* cosmological parameters are assumed, a value of $\Sigma\, m_\nu \simeq 0.34$ eV is required to fit with the data.

Key words: neutrinos – methods: numerical – galaxies: clusters: general – cosmology: theory – large-scale structure of Universe – X-rays: galaxies: clusters.

1 INTRODUCTION

The Standard Model (SM) of particle physics predicts the existence of three active neutrino species: the electron (ν_e), muon (ν_μ) and tau (ν_τ) neutrinos. These leptonic particles are chargeless and interact only via the weak force making them very elusive and difficult to study and leaving many open questions about their physical properties and on the possible existence of additional sterile species (see Mohapatra et al. 2007, for a review). While the SM originally assumed neutrinos to be massless, the discovery of leptonic flavour oscillations suggests that they have a non-zero mass, fixing the lower limit for the sum of neutrino masses to $\Sigma\, m_\nu \equiv m_{\nu_\mathrm{e}} + m_{\nu_\mu} + m_{\nu_\tau} \gtrsim 0.05$ eV[1] (see Lesgourgues & Pastor 2006, 2012, 2014; Lesgourgues et al. 2013; Gonzalez-Garcia 2014, and references therein). This opens the possibility to study neutrino properties also via their gravitational interaction.

From the cosmological point of view the presence of a thermal neutrino component has two important effects. First, since they become non-relativistic after the epoch of recombination they behave as an additional component in the radiation-dominated era, modifying the radiation density term

$$\rho_\mathrm{r} = \rho_\gamma + \rho_\nu = \left[1 + \frac{7}{8}\left(\frac{4}{11}\right)^{\frac{4}{3}} N_\mathrm{eff}\right]\rho_\gamma, \tag{1}$$

[1] More specifically, $\Sigma\, m_\nu$ must be greater than approximately 0.06 eV in the normal hierarchy scenario and 0.1 eV in the degenerate hierarchy.

★ E-mail: mauro.roncarelli@unibo.it

© 2014 The Authors
Published by Oxford University Press on behalf of the Royal Astronomical Society

Downloaded from http://mnras.oxfordjournals.org/ at INAF Brera Milano (Osservatorio Astronomico di Brera) on January 9, 2015

where ρ_γ and ρ_ν are the photon and neutrino energy densities, respectively, and $N_{\rm eff}$ is the effective number of neutrino species that according to the SM predictions should be fixed to $N_{\rm eff} = 3.046$. This has the effect of postponing the matter radiation equality for a given value of $\Omega_{\rm m} h^2$ (being $\Omega_{\rm m}$ the ratio between the matter density of the Universe and the critical one, $\rho_{\rm c}$, at $z = 0$ and h the Hubble constant H_0 in units of 100 km s^{-1} Mpc^{-1}) and modifying the background evolution, therefore slightly affecting the properties of the primary cosmic microwave background (CMB) anisotropies. In addition, after recombination neutrinos act as a hot dark matter (HDM) component whose energy-density parameter depends on the CMB temperature, $T_{\rm CMB}$, and $\Sigma\, m_\nu$ only:

$$\Omega_\nu \equiv \frac{\rho_\nu}{\rho_{\rm c}} = \frac{16\,\zeta(3)\,T_{\rm CMB}^3}{11\pi\,H_0^2}\,\Sigma\, m_\nu \simeq \frac{\Sigma\, m_\nu}{93.14\,h^2\,{\rm eV}}, \tag{2}$$

where[2] ζ is the Riemann zeta function, with $\zeta(3) \simeq 1.202$. Even if present CMB observations put strong constraints on the amount of HDM in the Universe, indicating that Ω_ν must be very small, this component can produce significant effects on the large-scale structure (LSS) evolution. In fact, the large thermal velocities of non-relativistic neutrinos suppress the growth of neutrino densities perturbations on scales smaller than their characteristic free-streaming comoving length:

$$\lambda_{{\rm fs},\nu} \simeq 7.67\,\frac{H_0(1+z)^2}{H(z)}\left(\frac{1\,{\rm eV}}{m_\nu}\right) h^{-1}\,{\rm Mpc}. \tag{3}$$

Since neutrinos induce a gravitational backreaction effect, also the evolution of both cold dark matter (CDM) and baryon (Rossi et al. 2014) density is affected and, therefore, the total matter power spectrum is hugely suppressed on such scales: this translates into a modification of the halo mass function (see e.g. Costanzi et al. 2013; Castorina et al. 2014; Villaescusa-Navarro et al. 2014). The dependence of equation (3) on the neutrino mass makes the growth of the LSS a sensitive tool to determine the value of $\Sigma\, m_\nu$ (see e.g. Viel, Haehnelt & Springel 2010; Marulli et al. 2011; Shimon et al. 2012; Carbone 2013; Costanzi Alunno Cerbolini et al. 2013; Mak & Pierpaoli 2013; Takeuchi & Kadota 2014).

Indeed, nowadays the tightest upper limits on the total neutrino mass come from cosmological studies. In detail, bounds have been put with Lyman α forest observations (e.g. Croft, Hu & Davé 1999; Viel, Haehnelt & Springel 2010), galaxy redshift surveys (Elgarøy et al. 2002; Tegmark et al. 2006; Thomas, Abdalla & Lahav 2010), CMB observations from the *Wilkinson Microwave Anisotropy Probe* (*WMAP*; Komatsu et al. 2009, 2011; Hinshaw et al. 2013), growth of galaxy clusters (Mantz, Allen & Rapetti 2010b; Mantz et al. 2015) and galaxy clustering (Zhao et al. 2013; Beutler et al. 2014; Sánchez et al. 2014). Currently, the most stringent upper limit comes from Riemer-Sørensen, Parkinson & Davis (2014) who combine the large-scale power spectrum from the WiggleZ Dark Energy Survey (Riemer-Sørensen et al. 2012) with CMB observations and measurements of the baryon acoustic oscillations (BAO) scale, yielding the upper limit of $\Sigma\, m_\nu < 0.18$ eV (95 per cent CL).

More recently the attention of the astrophysical community on this problem was raised by the *Planck* satellite observations. The cosmological results from the CMB anisotropies by Planck Collaboration XVI (2014) appear to be somewhat in tension with the ones from the thermal Sunyaev–Zel'dovich (SZ; Sunyaev & Zeldovich 1970) effect galaxy cluster survey obtained with the same instruments (Planck Collaboration XX 2014; Planck Collaboration XXIX 2014), while *Planck* CMB data (combined with *WMAP* polarization data and other high-resolution CMB experiments) constrain $\sigma_8(\Omega_{\rm m}/0.27)^{0.3} = 0.87 \pm 0.02$, being σ_8 the rms of matter density fluctuations in a sphere of $8\,h^{-1}$ Mpc at the present epoch, the galaxy cluster counts analysis indicates a significantly lower value of 0.78 ± 0.01, which translates into about a factor of 2 less objects detected than expected from the CMB analyses. If on one side the systematics connected with both the X-ray and SZ scaling-laws adopted (see e.g. Sereno, Ettori & Moscardini 2014) and the uncertainties in the modelling of non-thermal pressure bias (see e.g. the study on *Planck* clusters by von der Linden et al. 2014) may hamper the robustness of the SZ cluster findings, on the other hand these results are consistent with other measurements obtained from other galaxy cluster surveys at different wavelengths and affected by completely different systematics (Vikhlinin et al. 2009; Rozo et al. 2010; Hasselfield et al. 2013; Reichardt et al. 2013). Moreover, the low σ_8 scenario fits also with the expected number counts derived from the *Planck* y-parameter map analysis (Planck Collaboration XXI 2014). The presence of massive neutrinos offers a possible natural explanation of this apparent discrepancy between the high- and low-redshift universe, while CMB analyses assume a six free-parameter standard Λ cold dark matter (ΛCDM) cosmology, adding a small $\Sigma\, m_\nu$ as an additional component can help reconcile the discrepancy (see Battye, Charnock & Moss 2014; Costanzi et al. 2014, for a more detailed discussion on this topic). In the framework of this new ΛCDMν scenario Planck Collaboration XX (2014) obtained $\Sigma\, m_\nu = (0.20 \pm 0.09)$ eV with a joint analysis of *Planck*-CMB, *Planck*-galaxy clusters and BAO: if confirmed this result would represent the tightest constraint for neutrino masses up to date.

One of the main difficulties in using LSS probes to determine $\Sigma\, m_\nu$ is the degeneracy with the other cosmological parameters sensitive to the growth of cosmic structures, namely σ_8 and $\Omega_{\rm m}$. The key to break this degeneracy is either the combination of different observables that allow to determine its redshift evolution, or adding CMB priors to the analysis of LSS data. Carbone et al. (2011) showed that future spectroscopic galaxy surveys planned for the next decade, like *Euclid* (Laureijs et al. 2011) and *Wide-Field Infrared Survey Telescope* (*WFIRST*; Spergel et al. 2013), when combined with *Planck* priors will be able to measure both $N_{\rm eff}$ and $\Sigma\, m_\nu$ independently of the galaxy power spectrum normalization, the dark energy parametrization and the assumption of flat geometry if $\Sigma\, m_\nu > 0.1$ eV. Conversely, if $\Sigma\, m_\nu$ is lower, they will allow a measurement in the framework of a flat ΛCDM model. In the next years also galaxy clusters surveys will play an important role in this framework (Carbone et al. 2012; Costanzi Alunno Cerbolini et al. 2013). The South Pole Telescope (SPT) team, which has recently released a first catalogue of 224 galaxy clusters detected via SZ effect in an area of 720 deg^2 (Reichardt et al. 2013), is expected to achieve almost 1000 identifications with the full 2500 deg^2 survey, together with a measurement of the SZ power spectrum at the arcminute scale with unprecedented accuracy. In addition the *extended Roentgen Survey with an Imaging Telescope Array* (*eROSITA*) satellite (see Predehl et al. 2007; Merloni et al. 2012) will perform a full-sky survey in the X-rays with the potential of detecting about 10^5 galaxy clusters down to $z \approx 1$–1.5. Provided that these objects will have adequate redshift measurements, these data will improve significantly our knowledge of how the LSS evolves with time. This will allow not only an independent set of measurements of both $\Omega_{\rm m}$

[2] Equation (2) is expressed in Planck units, i.e. $G = \hbar = c = k_{\rm B} = 1$.

Downloaded from http://mnras.oxfordjournals.org/ at INAF Brera Milano (Osservatorio Astronomico di Brera) on January 9, 2015

Table 1. Set of parameters assumed in our six simulations. Second and third columns: density parameter of the cosmological constant and CDM, respectively, in per cent units. Fourth column: neutrino mass fraction, defined as $f_\nu \equiv \Omega_\nu/\Omega_m$, in per cent units. The values of Ω_Λ, Ω_{CDM} and Ω_ν are set to be consistent with a flat universe ($\Omega = 1$). From fifth to eighth column, respectively: sum of the neutrinos masses ($\Sigma\, m_\nu$), Hubble constant (H_0), normalization of the primordial power spectrum of the density fluctuations (A_S) and rms of matter density fluctuations in a sphere of $8\,h^{-1}$ Mpc (σ_8) at $z = 0$. The ninth column shows the number of particles used in the simulations (N_p) and the last two columns show the mass of the CDM and neutrino particles, respectively. For all simulations the comoving volume size is $(2\,h^{-1}\ \mathrm{Gpc})^3$.

Simulation	$10^2\,\Omega_\Lambda$	$10^2\,\Omega_{CDM}$	$10^2 f_\nu$	$\Sigma\, m_\nu$ (eV)	H_0 (km s^{-1} Mpc^{-1})	$10^9 A_S$	σ_8 ($z = 0$)	N_p	$m_{p,cdm}$ ($10^{10}\,h^{-1}\,M_\odot$)	$m_{p,\nu}$ ($10^{10}\,h^{-1}\,M_\odot$)
P0	68.39	31.61	0	0	67.11	2.15	0.834	1024^3	65.36	–
P17	68.39	31.20	1.30	0.17	67.11	2.15	0.794	2×1024^3	64.53	0.84
P34	68.39	30.80	2.56	0.34	67.11	2.15	0.751	2×1024^3	63.69	1.68
W0	72.90	27.10	0	0	70.3	2.43	0.809	1024^3	56.04	–
W17	72.90	26.73	1.37	0.17	70.3	2.43	0.767	2×1024^3	55.28	0.76
W34	72.90	26.36	2.73	0.34	70.3	2.43	0.723	2×1024^3	54.51	1.53

and σ_8, but has also the potential of providing useful constraints on $\Sigma\, m_\nu$.

In this work we study how massive neutrinos affect the SZ and X-ray observables of galaxy clusters and how the expected detections from upcoming galaxy cluster surveys will be influenced by both the value of $\Sigma\, m_\nu$ and by the uncertainty in other cosmological parameters. Like in our previous work on non-Gaussianities of primordial density fluctuations (Roncarelli et al. 2010), we use a set of six cosmological simulations that describe the formation of CDM structures including a massive neutrino component, with different values of $\Sigma\, m_\nu$ and in two different cosmological scenarios. Starting from high redshift, our simulations follow the evolution of a very large comoving volume of the Universe, namely $8\,h^{-3}$ Gpc^3, allowing us to achieve an accurate description of the mass function up to the highest mass haloes, well above $10^{15}\,M_\odot$. After identifying galaxy clusters in our simulation outputs, we use scaling relations derived from observations to link their masses with their SZ and X-ray observables. By considering the geometry derived from the corresponding cosmological model, we associate to each halo a position in the sky, reconstruct the past light cones of the LSS and create mock y-parameter observational maps. We compare our results with *Planck* observations, both for cluster counts and for the y-parameter power spectrum, and provide forecasts for future SPT and *eROSITA* cluster surveys.

This paper is organized as follows. In the next section we describe the characteristics of the simulation set used for this work, the algorithms used to identify the haloes and our method for the light cone reconstruction. In Section 3 we describe the model used to associate the SZ signal to each halo and discuss our results on the effect of neutrino mass on number counts and SZ power spectrum. In Section 4 we discuss the aspects connected with the X-ray properties of galaxy clusters and provide forecasts on the possible detections by *eROSITA*. We summarize and draw our conclusions in Section 5. For the purpose of our work we will use two different cosmological models with different values of the Hubble parameter h. However in order to provide a consistent comparison we will fix $h = 0.7$ ($h_{70} = 1$) for both models whenever describing the predicted observational properties.

2 MODELLING THE EFFECT OF NEUTRINOS ON THE LSS

2.1 The simulation set

For this work we use a set of cosmological simulations performed with the tree particle mesh–smoothed particle hydrodynamics (TreePM–SPH) code GADGET-3, an evolution of the original code GADGET (Springel 2005) specifically modified by Viel et al. (2010) to account for the neutrino density evolution. Here we summarize the characteristics of the code and we refer to the original work for the details (see also Bird, Viel & Haehnelt 2012; Villaescusa-Navarro et al. 2013, 2014). The code follows the evolution of CDM and neutrino particles treating them as two separated collisionless fluids. Given the relatively higher velocity dispersion, neutrinos have a characteristic clustering scale larger than the CDM one, allowing to save computational time by neglecting the calculation of the short-range gravitational force. This results in a different spatial resolution for the two components: fixed by the PM grid for neutrinos and about one order of magnitude higher for CDM.

Starting from initial conditions with the same random phases, we run a total of six different cosmological simulations on very large scales, following a comoving volume of $(2\,h^{-1}\ \mathrm{Gpc})^3$ from $z = 99$ to present epoch, filled with 1024^3 dark matter particles and, where present, an equal amount of neutrino particles. No baryon physics is included in these simulations. We choose the cosmological parameters of the first three simulations, dubbed P0, P17 and P34, according to the *Planck* results (Planck Collaboration XVI 2014), namely a flat ΛCDM model which we generalize to a ΛCDMν framework by changing only the value of the sum of the neutrino masses $\Sigma\, m_\nu = (0, 0.17, 0.34)$ eV, respectively, and keeping fixed Ω_m and the amplitude of primordial scalar perturbations A_S. For the other simulation set (W0, W17 and W34) we assume the baseline ΛCDM cosmology derived from the 9-year results of the *WMAP* satellite (Hinshaw et al. 2013), and introduce massive neutrinos with masses $\Sigma\, m_\nu = (0, 0.17, 0.34)$ eV in the same way. For each simulation we produced 64 outputs logarithmically equispaced in the scale factor $a = 1/(1 + z)$, in the redshift interval $z = 0$–99. The list of cosmological and numerical parameters assumed for the two simulation sets is reported in Table 1.

2.2 Halo identification

First, we process the simulation outputs with the friends-of-friends (FoF) algorithm included in the GADGET-3 package. The code is applied only to CDM particles with linking length fixed to 0.16 times the mean interparticle distance. The minimum number of particles to identify a structure is set to 32, thus fixing its minimum mass to $M_{FoF} \simeq 2 \times 10^{13}\,h^{-1}\,M_\odot$. Neutrino particles are subsequently attached to a given parent halo if the closest CDM particle belongs to it. The FoF catalogues are then processed with the SUBFIND algorithm (Springel et al. 2001; Dolag et al. 2009) included in the GADGET-3 package, which identifies locally overdense

Downloaded from http://mnras.oxfordjournals.org/ at INAF Brera Milano (Osservatorio Astronomico di Brera) on January 9, 2015

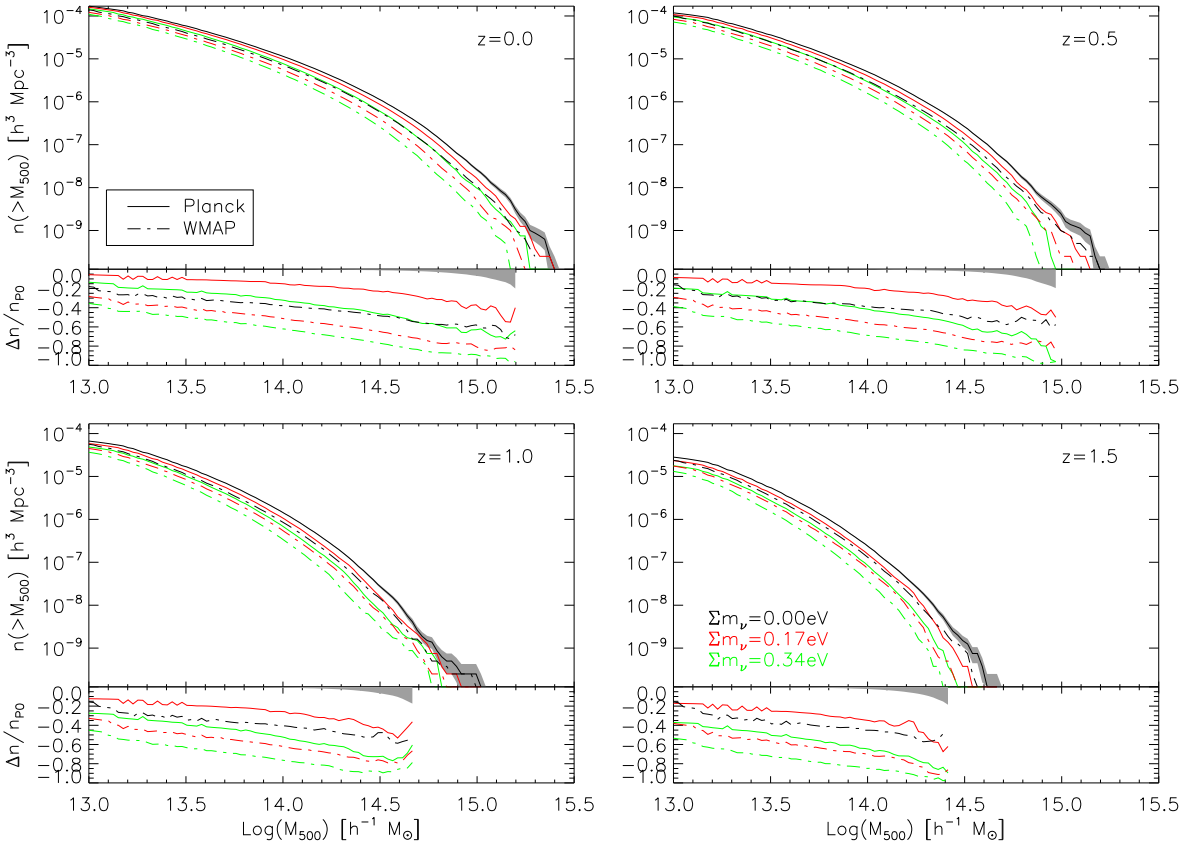

Figure 1. Upper subpanels: mass function, in terms of comoving number density of haloes above a given M_{500}, for the two simulation sets at different redshifts. Solid lines refer to the Planck simulation set (P0, P17, P34), dot–dashed lines refer to the WMAP simulation set (W0, W17, W34). The three different values of $\Sigma\, m_\nu = (0, 0.17, 0.34)$ eV are shown in black, red and green, respectively. In the lower subpanels we show the fractional differences $\Delta n/n$, with respect to the P0 simulation. The grey shaded area encloses the Poissonian error computed over the simulation volume for the P0 model only.

gravitationally bound regions within an input parent halo. Here we adopt a minimum number of 20 particles to make a valid subhalo. Moreover, we use a specific routine included in the SUBFIND algorithm to compute spherical overdensities for FoF groups, and, in particular, for each halo we compute the value of R_{500}, defined as the radius enclosing a matter (CDM+neutrinos) density equal to 500 times the critical density of the Universe $\rho_c(z)$ at the cluster redshift, and the corresponding mass in terms of $M_{500} \equiv 500\rho_c(z) \times \frac{4}{3}\pi R_{500}{}^3$. The choice of the density contrast $\delta = 500$ is done in order to simplify the use of scaling relations to compute observables (see Sections 3 and 4). We stress also that the density threshold adopted in our study is significantly higher with respect to other works (see e.g. Villaescusa-Navarro et al. 2014): this makes the contribution of the neutrino component to the total mass of the subhaloes negligible. With this procedure some of the initial FoF parent haloes are split into multiple subhaloes, with the result of an increase of the total number of identified objects and of a lower minimum mass limit.

We show in Fig. 1 the mass functions of our six simulations in terms of number density of haloes above a given M_{500} at four different redshifts. As expected, the presence of massive neutrinos slows down structure formation resulting in a smaller number of haloes per fixed mass at all redshifts. When looking at the $z = 0$ plot, in the mass range $M_{500} = 10^{13.5\text{–}14.5}\, h^{-1}\, \mathrm{M}_\odot$ the P17 model shows about 10–20 per cent less haloes than the P0 one, with differences doubled when considering the P34 and P0 models. Similar differences are found for the WMAP simulation set. We can also observe that the action of massive neutrinos is not completely degenerate with respect to the remaining cosmological parameters if we take into account the redshift evolution and the shape of the mass function. More precisely, the decrease in the number of haloes due to neutrino free-streaming shows a steeper dependence on both mass and redshift.

Massive neutrinos affect also the clustering of LSSs, as shown by the two-point spatial autocorrelation function of haloes in Fig. 2. Differently from the mass function case, massive neutrinos enhance halo clustering and the value of ξ at all scales and redshifts (see the discussion in Marulli et al. 2011). Considering the Planck simulation set, we observe that massive neutrinos produce a 20 per cent increase of the value of ξ for the P34 simulation with respect to the P0 one, independent of scale and almost independent of redshift up to $z = 1$. Similar differences are found in the WMAP simulation set. On the other side, the increase of the value of ξ associated with the baseline cosmology is significantly higher: the W0 simulation shows a 20 per cent higher correlation than the P0 one at small scales, with differences increasing with distance up to 40 per cent at $50\, h^{-1}$ Mpc. This indicates that the use of cluster counts and cluster correlation function can help to break the degeneracy between neutrino mass and cosmological parameters (see also the discussion in Sánchez et al. 2014).

2.3 Light cone construction

The method to create the past light cones from the simulation outputs is similar to the one described in our previous works (see Roncarelli et al. 2006a, 2007, 2010, 2012). The procedure

Downloaded from http://mnras.oxfordjournals.org/ at INAF Brera Milano (Osservatorio Astronomico di Brera) on January 9, 2015

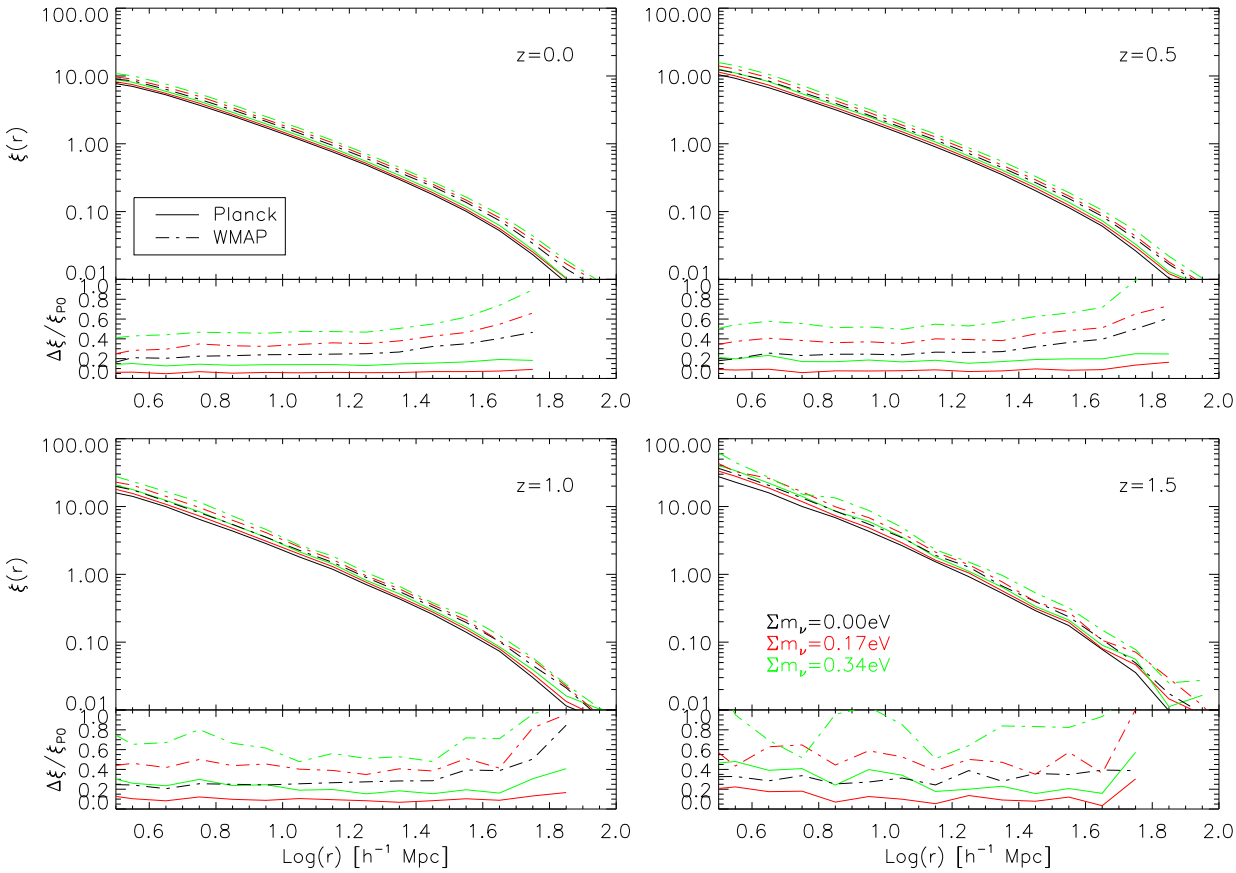

Figure 2. Two-point spatial autocorrelation of haloes ($M_{500} > 10^{13.5}\,h^{-1}\,\mathrm{M}_\odot$) as a function of comoving distance for the two simulation sets at different redshifts. Lines and colour coding are the same as in Fig. 1. In the lower subpanels we show the fractional differences $\Delta\xi/\xi$, with respect to the P0 simulation.

consists in stacking the different simulation volumes along the line of sight, down to a redshift limit that we fix for our purposes to $z = 3$, corresponding to 4381 h^{-1} (4601 h^{-1}) comoving Mpc for the *Planck* (*WMAP*) baseline cosmology, thus requiring to stack three times the simulation volume to fill up the light cone. In order to exploit the full redshift sampling of the simulation outputs, each simulation volume is divided into slices along the line of sight to which we assign a different snapshot. The interval corresponding to the different slices is chosen by computing the age of the Universe as a function of the comoving distance from the observer and by assigning to each slice the snapshot that better matches this quantity. Given our set of snapshots we obtain 39 slices for both simulation sets.

In order to avoid the superimposition of the same structures along the line of sight, every simulation box undergoes a randomization process that consists of four steps: (i) we assign a 50 per cent probability to reflect each side of the output; (ii) we randomly choose the axis to be oriented along the line of sight and the direction of the other two; (iii) we perform a random recentring of the spatial coordinates by exploiting the periodic boundary conditions and (iv) we rotate the cube along the line of sight choosing a random angle. The slices belonging to the same cube volume undergo the same randomization process in order to preserve the large-scale power information. We repeat this process using the same random seeds for our six simulations: this, together with the use of the same phases in the initial conditions, ensures that we represent the same comoving volume with six different cosmological models, reducing the impact of cosmic variance on our results.

We fix the opening angle of each light cone to 10° per side, a limit that ensures the validity of the flat-sky approximation, enclosing a comoving volume of 0.854 (0.977) h^{-3} Gpc^3 for the Planck (WMAP) simulation set. By varying the initial random seed we generate 50 different light cone realizations that we use to assess the statistical robustness of our results, thus covering a total area of 5000 deg^2. Despite the very large size of our simulation volume, this total area cannot be considered completely independent. In fact, the projected comoving size of the simulation at $z = 3$ corresponds for the Planck (WMAP) model to 681 (622) deg^2, indicating that at the end of the light cone we are replicating the same structure about 7 (8) times. However in the redshift range $0 < z < 0.6$, where most of the X-ray and SZ signal is expected, the simulation size covers all of the 5000 deg^2, allowing us to consider the comoving volume of our 50 light cones as practically independent up to $z = 0.6$.

3 MODELLING THE SZ SIGNAL

Starting from the simulation outputs, we associate to each halo a value of the integrated Compton y-parameter Y_{500} as a function of M_{500} and z, using the scaling law adopted by Planck Collaboration XX (2014):

$$\frac{Y_{500}}{\mathrm{arcmin}^2} = E^{\beta}(z)\,\frac{10^{-4}\,Y_*}{6^{\alpha}}\left(\frac{h_{70}^{-1}\,\mathrm{Mpc}}{d_{\mathrm{A}}(z)}\right)^2\left[\frac{(1-b)M_{500}}{10^{14}\,h_{70}^{-1}\,\mathrm{M}_\odot}\right]^{\alpha}, \quad (4)$$

where $E(z) \equiv H(z)/H_0 = \sqrt{\Omega_{\mathrm{m}}(1+z)^3 + \Omega_\Lambda}$, β is fixed to the self-similar evolution value of 2/3 and $d_{\mathrm{A}}(z)$ is the angular

Downloaded from http://mnras.oxfordjournals.org/ at INAF Brera Milano (Osservatorio Astronomico di Brera) on January 9, 2015

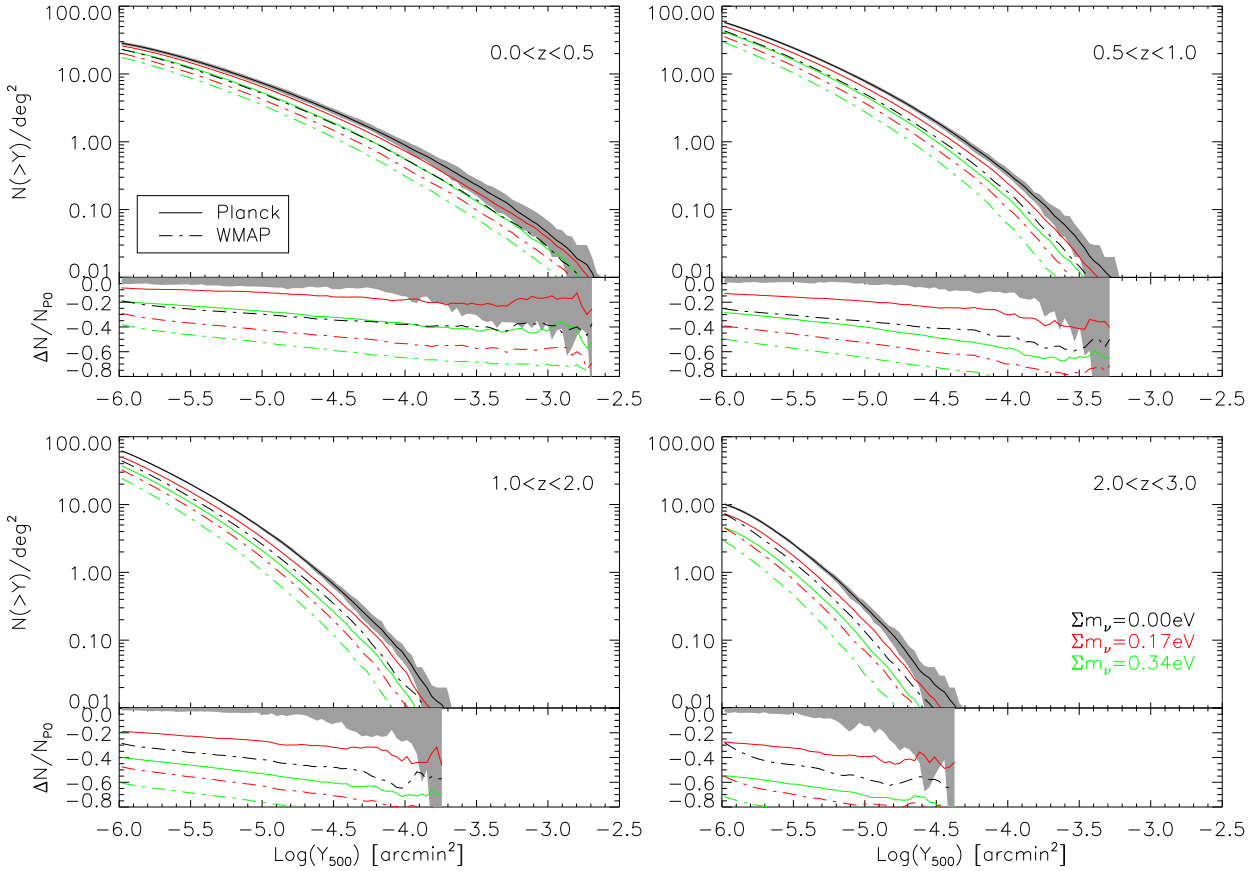

Figure 3. Number of haloes per square degree as a function of the limit in Y_{500}. Lines and colour coding are the same as in Fig. 1, the grey shaded area encloses the central 68 per cent of the values computed in the 50 different light cones (100 deg^2 each) for the P0 model.

diameter distance. The quantities Y_*, α and b (normalization, slope and pressure bias, respectively) are taken from the baseline values of Planck Collaboration XX (2014) and fixed to 0.646, 1.79 and 0.2, respectively, for all haloes. Once the expected value of Y_{500} is computed, the final value is determined by adding randomly an intrinsic scatter with a logarithmic standard deviation $\sigma_{\mathrm{Log}Y} = 0.075$.

Under these assumptions we compute the expected number of haloes above a given Y_{500} in different redshift bins, and show the results in Fig. 3. The differences are comparable to what observed in Fig. 1 for the mass function, with decrements in the expected number counts roughly proportional to the value of $\Sigma\, m_\nu$. We can see, however, that while at low redshift the W0 model appears almost degenerate with the P34 one, when moving towards higher redshift the effect of neutrinos is stronger. The cosmic variance (grey shaded area) computed as the interval that encloses the central 68 per cent of the values in the 50 different fields is smaller than the difference between the various models for $Y_{500} \lesssim 10^{-4}$ arcmin^2 and approximately follows Poissonian statistics.

We use our models also to predict the expected detections by the SPT and *Planck* surveys. In general, the probability of detecting a galaxy cluster via the SZ effect depends not only on its Y_{500} value but also on the sky surface occupied by the halo: the latter determines the amount of noise, mainly primary CMB, and grows approximately linearly with the halo angular size. From the simulated light cone catalogues we derive the value of $\theta_{500} = \arcsin(R_{500}/d_{\mathrm{A}})$ for our objects. Then by using simulated data of SPT noise (Saro & Liu, private communication) we compute a value of ΔY that we use as a noise estimate and fix a signal-to-noise ratio (S/N) detection

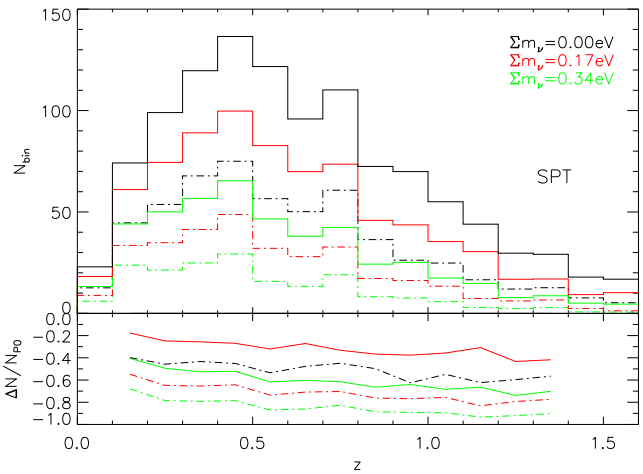

Figure 4. Predicted number counts in different redshift bins ($\Delta z = 0.1$) of galaxy clusters detectable by SPT (assuming S/N > 4.5 and a survey area of 2500 deg^2) for the two sets of simulations described in the text. Lines and colour coding are the same as in Fig. 1. In the lower panel we show the fractional difference computed with respect to the P0 simulation.

threshold of 4.5 (see Reichardt et al. 2013). Finally, we associate to each halo a detection probability by taking into account the intrinsic scatter in the Y_{500}–M_{500} relation of equation (4). We show in Fig. 4 the expected number of detections for the full SPT cluster survey (area of 2500 deg^2). We find that a value of $\Sigma\, m_\nu = 0.17$ eV reduces

Downloaded from http://mnras.oxfordjournals.org/ at INAF Brera Milano (Osservatorio Astronomico di Brera) on January 9, 2015

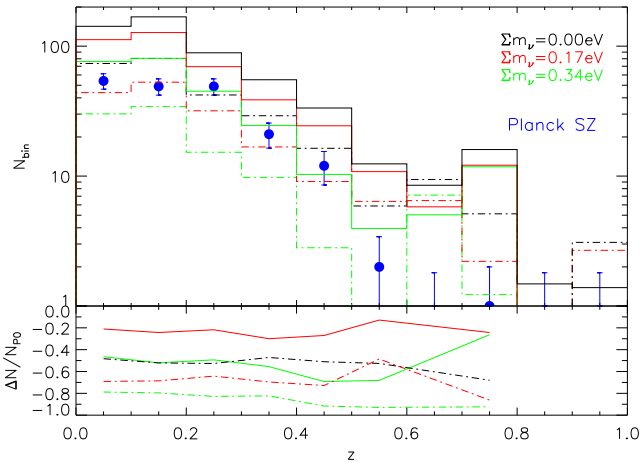

Figure 5. Same as Fig. 4 but for galaxy clusters detectable by *Planck* (see text for details). The blue points represent the detections by Planck Collaboration XX (2014) with 1σ error bars.

the expected detections by 20 per cent at $z = 0$ and up to 40 per cent at $z > 1$ with respect to the ΛCDM scenario in the *Planck* baseline cosmology. We can also see that for all models 15–20 per cent of the total detections will be at $z > 1$, where the neutrinos produce the largest differences. However the effect of neutrinos is almost degenerate with cosmology: in fact, the P34 and W0 models produce very similar results. This indicates that the SPT cluster survey alone will not be able to break the degeneracy between $\Sigma\, m_\nu$ and σ_8, and that a combination with data from other probes will be required to measure $\Sigma\, m_\nu$ precisely.

To obtain the estimate for the *Planck* cluster survey with an equivalent procedure we would need a precise and complete instrumental noise information which is not publicly available at the moment. For this reason we proceed in the following way. We consider the mass selection functions, $M_{\rm lim}(z)$, published by Planck Collaboration XX (2014, see their fig. 3) for the shallow, medium and deep surveys. Then for every halo in our catalogue we compute a detection probability $\chi(M_{500}, z)$. Since this quantity actually depends on Y_{500}, which is related to M_{500} with an intrinsic logarithmic scatter $\sigma_{{\rm Log}Y}$, we consider this effect by computing it in the following way:

$$\chi(M_{500}, z) = \sum_{i=1}^{3} \frac{f_i}{2} \left[1 + {\rm erf} \left(\frac{{\rm Log}\left(\frac{M_{500}}{M_{{\rm lim},i}(z)}\right)}{\sqrt{2}\sigma_{{\rm Log}Y}} \right) \right], \quad (5)$$

being f_i the area fraction of the three surveys (48.7, 47.8 and 3.5 per cent for the shallow, medium and deep surveys, respectively) and $M_{{\rm lim},\,i}(z)$ the relative selection function. Finally, for each cluster in our light cones we sum their individual detection probability and compute the expected number of detections per redshift bin considering a coverage area of 26 814 deg^2 (i.e. the 65 per cent of the full sky). We note, however, that our prediction for the P0 model is higher by about 30 per cent with respect to the equivalent one in Planck Collaboration XX (2014): we verified that this translates in a 10 per cent difference in the mass limit and is likely due to the approximations in our modelling of the *Planck* selection function. To overcome this problem, we apply this correction factor to the value of $M_{{\rm lim},\,i}(z)$ as it appears in equation (5). The corresponding results in terms of clusters number counts are plotted in Fig. 5. All the models that adopt *Planck* cosmology show an excess in the first two bins with respect to the real *Planck* detections (blue points), while at $z > 0.2$ the P34 model is in agreement with the data: this is consistent with what found by Planck Collaboration XX (2014) who obtain a value of $\Sigma\, m_\nu = (0.53 \pm 0.19)$ when considering CMB and clusters together. However this appears to be somewhat in tension with the result of $\Sigma\, m_\nu = (0.20 \pm 0.09)$ obtained when adding BAO data. Again, we observe that with respect to number counts the P34 and W0 model are almost perfectly degenerate.

We now analyse our predictions for the average y-parameter value and SZ power spectrum. By using our light cone catalogues, and under the assumption of clusters' spherical symmetry and of a fixed pressure profile, we are able to produce a set of mock y-parameter maps for each light cone realization and for each simulation, and use them to predict global SZ properties. Starting from the position of the cluster centres in the light cones, we assign to each object a projected pressure profile using a modification of the classic β-model (Cavaliere & Fusco-Femiano 1978), namely a rolling β polytropic profile that allows for a steepening of the density and temperature profiles in the outskirts (see Ameglio et al. 2006; Roncarelli et al. 2006b, 2010, and discussions therein). The profile, expressed in terms of the y-parameter, has the following form:

$$y(\theta) = \left[1 + \left(\frac{\theta}{\theta_{\rm c}} \right)^2 \right]^{(1-3\,\gamma\,\beta_{\rm eff})/2}, \quad (6)$$

where $\theta_{\rm c}$ is the angular size of the core radius, γ is the polytropic index of the gas, fixed to 1.18, and $\beta_{\rm eff}$ is the effective slope, defined as

$$\beta_{\rm eff} \equiv \frac{\beta_{\rm int} + \left(\frac{\theta}{\theta_{\rm c}}\right) \beta_{\rm ext}}{1 + \frac{\theta}{\theta_{\rm c}}}, \quad (7)$$

where $\beta_{\rm int}$ and $\beta_{\rm ext}$ represent the internal and external slopes of the profile, respectively. This method has the advantage of providing directly the projected quantity to map, with three free parameters, namely $\beta_{\rm int}$, $\beta_{\rm ext}$ and the ratio $\theta_{\rm c}/\theta_{500}$, that can be tuned to reproduce a given pressure profile. In particular we find the parameters values ($\beta_{\rm int} = 0.98$, $\beta_{\rm ext} = 1.28$ and $\theta_{\rm c}/\theta_{500} = 0.426$) that match the projection of the universal pressure profile of Arnaud et al. (2010) and apply them to our clusters. Given the high pressure contribution coming from external regions, we map the structure of our haloes up to 8 R_{500}.

We show in Fig. 6 the maps of the y-parameter obtained with this method for the same light cone realizations produced with the six simulations described in Table 1. These maps represent the whole 100 deg^2 sky patch after cutting out haloes whose centre is located at $z < 0.03$. We note that, even reproducing the same light cone volume in the six simulations (see Section 2.3), a significant cosmic variance from field to field is present, mainly due to the intrinsic scatter in the Y_{500}–M_{500} relation. It is clear from these images that the diminished abundance translates into a lower Comptonization value with increasing neutrino mass and moving from *Planck* to *WMAP* cosmology. We show in Table 2 the average y-parameter computed over the whole 5000 deg^2. The quoted error represents the 1σ deviation of the 50 different fields, i.e. the range that encloses the central 68 per cent of the values. First of all we must consider that these values are low when compared to other estimates obtained from hydrodynamical simulations, due to the lack of the diffuse component (i.e. filaments) which is expected to provide about half of the contribution to the whole integrated value (see the discussion in Roncarelli et al. 2007): this means that we have to consider these results as representative of the fraction of the expected total value associated with galaxy clusters only. As expected, massive neutrinos reduce consistently the average y-parameter, with P17 and P34 simulations having values about 20 and 40 per cent lower,

Downloaded from http://mnras.oxfordjournals.org/ at INAF Brera Milano (Osservatorio Astronomico di Brera) on January 9, 2015

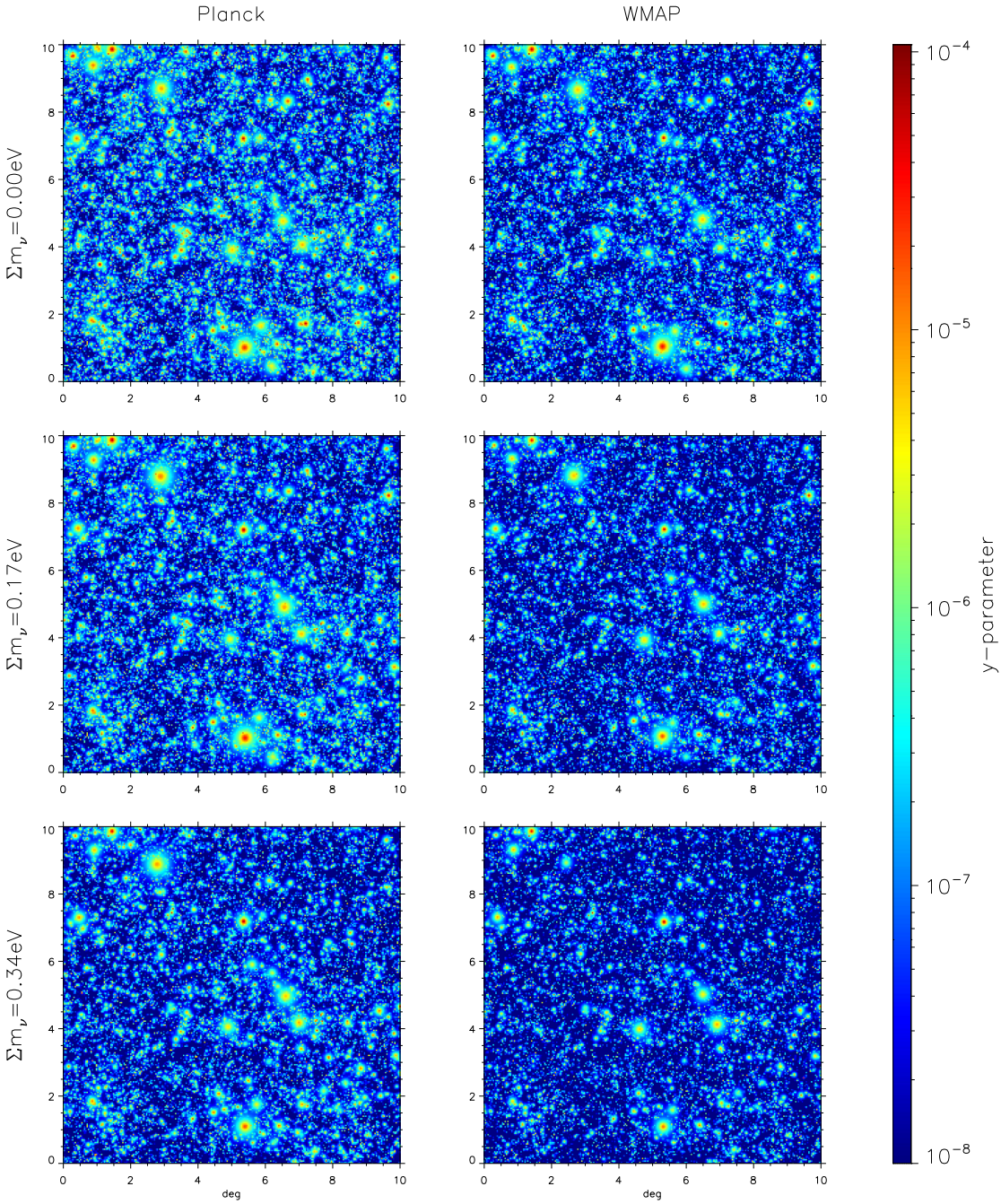

Figure 6. Maps of the y-parameter for the same light cone in our six models. Left- and right-hand columns correspond to the Planck and WMAP simulation set, respectively. Top, middle and bottom rows show the maps for $\Sigma\, m_\nu = (0, 0.17, 0.34)$ eV, respectively. Each map is 10° per side and considers all haloes with $z > 0.03$. All maps adopt the same colour scale, displayed on the right.

respectively, with respect to the P0 model. When considering the WMAP simulation set, the reduction is even higher (25 and 45 per cent for W17 and W34, respectively), due to the higher value of the ratio f_ν. Considering the whole set of six simulations we observe that the average y-parameter due to galaxy clusters scales as

$$\frac{\langle\, y_\nu \,\rangle}{\langle\, y_0 \,\rangle} \approx (1 - f_\nu)^{20}\,. \tag{8}$$

Another important quantity that can be used to observe the effect of neutrinos on the LSS of the Universe is the SZ power spectrum, which is known to be the dominant source of CMB anisotropies at small scales ($\lesssim$5 arcmin) and that has been recently measured by *Planck* (Planck Collaboration XXI 2014), SPT (Reichardt et al. 2012; Crawford et al. 2014) and Atacama Cosmology Telescope (ACT; Sievers et al. 2013). Using the complete set of y-parameter maps (six maps like the ones of Fig. 6 for each light cone realization) we compute their power spectrum with a method based on fast Fourier transform and in the flat-sky approximation, and express it in terms of power as a function of the multipole ℓ.

Since for each model the power spectrum shows significant changes from one light cone to another due to the cosmic variance,

Downloaded from http://mnras.oxfordjournals.org/ at INAF Brera Milano (Osservatorio Astronomico di Brera) on January 9, 2015

Table 2. Average y-parameter in the whole simulation set. The quoted error encloses the central 68 per cent of the values of the 50 light cones. These values do not account for the diffuse component, e.g. the gas outside galaxy clusters.

Simulation	$\langle y \rangle\,(10^{-7})$
P0	$4.82^{+0.45}_{-0.37}$
P17	$3.92^{+0.32}_{-0.29}$
P34	$2.95^{+0.20}_{-0.19}$
W0	$3.23^{+0.25}_{-0.21}$
W17	$2.41^{+0.17}_{-0.17}$
W34	$1.84^{+0.15}_{-0.14}$

Table 3. Properties of the SZ power spectrum for our six simulations. From second to fourth column: values of the best-fitting parameters (see text for details) to the simulated data using equation (9). The fifth column indicates the value of the best-fitting function at $\ell = 3000$, with the errors that represent the interval enclosing the central 68 per cent of the values of the 50 different light cone realizations. The values A and A_{3000} are expressed in terms of $(\Delta T/T_{\rm CMB})^2$ in the RJ limit.

Simulation	$A\,(10^{-12})$	μ	σ	$A_{3000}\,(10^{-12})$
P0	6.84	3.90	0.692	$5.27^{+1.16}_{-1.01}$
P17	5.03	3.91	0.700	$3.84^{+0.75}_{-0.68}$
P34	3.38	3.90	0.706	$2.55^{+0.44}_{-0.54}$
W0	3.58	3.92	0.685	$2.77^{+0.54}_{-0.53}$
W17	2.33	3.93	0.693	$1.78^{+0.38}_{-0.35}$
W34	1.54	3.95	0.678	$1.19^{+0.23}_{-0.24}$

in order to define a global quantity for each simulation we proceed in the following way. For every simulation and for each value of the multipole ℓ we consider the values of $P(\ell) \equiv \ell(\ell+1)C_\ell/(2\pi)$ obtained in the 50 different light cones and, after defining $x \equiv \mathrm{Log}(\ell)$, we compute the average $P(x)$ for each model and we quantify their dispersion by considering the eight highest and eight lowest values and by defining $\sigma(\ell)$ as the half of their difference. Then, we observe that the result can be fit with a skew-normal distribution (Azzalini 1985) with shape parameter fixed[3] to $\alpha = -\sqrt{2}$, thus with the following formula:

$$P(x) = \frac{A}{\sqrt{2\pi}\,\sigma}\,\exp\left(-\frac{(x-\mu)^2}{2\sigma^2}\right)\left[1+\mathrm{erf}\left(\frac{\mu - x}{\sigma}\right)\right], \qquad (9)$$

where A, μ and σ are left as free parameters. Finally, for each model we fit the average power spectrum by using the value of $\sigma(\ell)$ as an error for each point. We report in Table 3 the best-fitting parameters for each model and plot in Fig. 7 the corresponding SZ power spectra in the Rayleigh–Jeans (RJ) limit. For all the models the peak position, defined by the μ parameters show small changes. On the other hand, the *WMAP* models show slightly lower values of σ and, most importantly, the normalization is highly influenced by the presence of massive neutrinos: the P17 and W17 models show a reduction of 25–30 per cent with respect to the corresponding ΛCDM model, while for the P34 and W34 models the normalization is reduced to less than a half. We find that its dependence on f_ν scales approximately as

$$\frac{A_\nu}{A_0} \approx (1-f_\nu)^{25-30}\,. \qquad (10)$$

Our results can be compared to the measurements at $\ell < 1000$ of Planck Collaboration XXI (2014) and to the ones at $\ell = 3000$ of SPT (Reichardt et al. 2012; Crawford et al. 2014) and ACT (Sievers et al. 2013), also plotted in Fig. 7. As a reference, we also show in Table 3 the value of A_{3000} for our six models in the RJ limit.[4] We can see that none of our models is able to reproduce the flattening obtained by *Planck* at large scales, resulting in a significant underestimate of the measured spectrum at $\ell \lesssim 200$: this is likely due to the lack in our model of the diffuse component associated with non-virialized structures. The points at $\ell \gtrsim 200$ are well fitted by our P17 model, with also the P34 and W0 providing acceptable fits to the data. Considering the uncertainty due to the cosmic variance, this is in broad agreement with the result of Planck Collaboration XXI (2014), who obtain best-fitting values of $\sigma_8 = 0.74 \pm 0.06$ and $\Omega_{\rm m} = 0.33 \pm 0.06$. On the other hand, the results at $\ell = 3000$ favour the P34, W0 and W17 models which are all consistent at about 1σ. The P17 model shows an excess at more than 3σ with respect to both SPT measurements and at 2σ with respect to ACT data: this highlights a general difficulty of this kind of models fitting both low and high ℓ measurements of the SZ power spectrum.

4 MODELLING X-RAY COUNTS

In this section we aim at describing the X-ray properties of the galaxy clusters in our simulations and predicting the expected number counts for the *eROSITA* all-sky survey, that will constitute an important probe of the LSS in the next future. However, this kind of modelling is significantly more difficult than the corresponding SZ one, mainly due to the uncertainties associated with the X-ray scaling laws and to their redshift evolution, making our results uncertain in terms of absolute values. For this reason, we focus on the discussion of the relative differences associated with the presence of massive neutrinos, that are less dependent on our model assumptions.

In order to assign to each galaxy cluster an X-ray luminosity we adopt the scaling law of Mantz et al. (2010a), namely

$$\frac{L_{500}}{10^{44}\,h_{70}^{-2}\,\mathrm{erg\,s^{-1}}} = E(z)10^{\beta_0}\left(\frac{E(z)\,M_{500}}{10^{15}\,h_{70}^{-1}\,\mathrm{M_\odot}}\right)^{\beta_1}, \qquad (11)$$

where L_{500} is the bolometric X-ray luminosity inside R_{500}, and the two parameters β_0 and β_1 are fixed to their best-fitting values of 1.23 and 1.63, respectively. Here we are assuming a self-similar redshift evolution. After computing the expected value of L_{500} we also apply an intrinsic logarithmic scatter characterized by $\sigma_{\mathrm{Log}L} = 0.17$. We then convert each bolometric luminosity to the corresponding flux in the 0.5–2 keV band:

$$S_{[0.5-2]} = \frac{L_{500}\,f(T_{500}, z)}{4\pi\,d_L^2(z)}, \qquad (12)$$

where $d_L(z)$ is the luminosity distance, $f(T_{500}, z)$ is the band correction, computed assuming a bremsstrahlung emission. The cluster

[3] This value is chosen to simplify the expression in equation (9) and corresponds to a skewed Gaussian curve, with skewness equal to −0.272.

[4] To obtain the corresponding values at 150 GHz (SPT) and 148 GHz (ACT) one should divide our results by a factor of 4.40 and 4.17, respectively.

Downloaded from http://mnras.oxfordjournals.org/ at INAF Brera Milano (Osservatorio Astronomico di Brera) on January 9, 2015

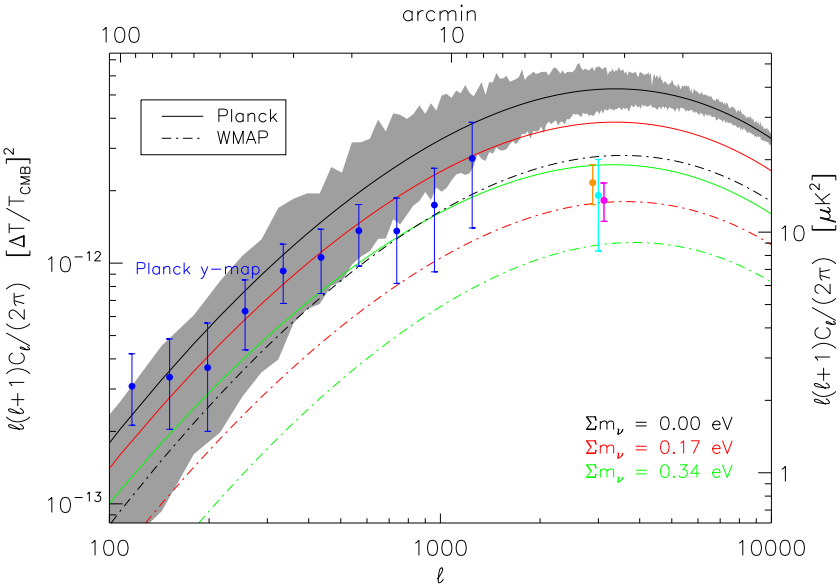

Figure 7. Power spectrum of the SZ signal in the RJ limit as a function of the multipole ℓ for the two simulation sets. Lines and colour coding are the same as in Fig. 1. All these lines represent the average over the 50 light cone realizations, while the grey shaded area encloses the 1σ deviation between the 50 light cones for the P0 simulation only (see text for details). The blue points represent the SZ power spectrum measurements by *Planck* (Planck Collaboration XXI 2014). The orange and magenta points represent the SPT results by Reichardt et al. (2012) and Crawford et al. (2014), respectively. The cyan point represents the ACT measurement by Sievers et al. (2013).

temperature T_{500} is also computed applying the scaling law obtained by Mantz et al. (2010a) and assuming a self-similar redshift evolution.

Under these assumptions we compute the number of clusters detectable by the *eROSITA* full-sky survey by adopting a simple flux threshold of 3×10^{-14} erg s^{-1} cm^{-2} in the 0.5–2 keV band, as reported in Merloni et al. (2012). We stress that the problem of determining the actual detectability of a galaxy cluster in the real survey is a more complicated issue, connected to the capability of disentangling faint cluster candidates from contaminating sources [mainly faint active galactic nuclei (AGN) at high redshift] given the large point spread function (PSF) of *eROSITA* (see e.g. a discussion on this problem with *XMM–Newton* observations in Brusa et al. 2010), which is beyond the scope of this paper. For this reason our results should be interpreted as upper limits of the *eROSITA* survey capability.

We show in Fig. 8 the $\log N$–$\log S$ of the haloes in our 50 light cones. These results look similar with what already said for Fig. 3, with the inclusion of massive neutrinos causing comparable decrements in the expected number of haloes. In this case the different redshift evolution of the X-ray flux makes the degeneracy with respect to cosmology more severe, especially between the P34 and W0 models at all redshifts. This is mainly due to the value of the $\Omega_{\rm m}$ parameter that influences the redshift evolution through $E(z)$ (see equation 11).

The potential of the *eROSITA* survey comes out more clearly when analysing the expected detections in the redshift bins shown in Fig. 9. For this computation we considered only haloes with $M_{500} > 10^{14}\,h^{-1}\,{\rm M}_\odot$, in order to avoid further uncertainties in the scaling relations adopted. With our assumptions the *eROSITA* cluster survey would be almost volume limited for the haloes above this mass. The total number of potential detections for the P0 model is about 180 000, which is consistent with what quoted by Merloni et al. (2012). This makes the differences associated with a change in the value of $\Sigma\, m_\nu$ highly significant in terms of the corresponding Poissonian uncertainties in all redshift bins.

Given the very high number of potential detections we can compute the corresponding angular correlation function $w(\theta)$ for the six models considered in this work and check if it can break the degeneracy between $\Sigma\, m_\nu$ and cosmology, as said in Section 2.2. The results plotted in Fig. 10 show a trend similar to what happens for the cluster correlation function shown in Fig. 2, with a higher correlation for *WMAP* cosmology and for higher neutrino masses, with differences that are larger than the typical Poissonian error at $\theta \gtrsim 10$ arcmin. However, even if the fractional differences are high, the value of $w(\theta)$ at these angular scales is small (below 0.1 for all models), indicating that the systematics associated with the scaling law, and in particular to the redshift evolution, will dominate the uncertainty making it difficult to disentangle between the different models. This indicates that in order to exploit the correlation function a good control of observational systematics is required, together with precise mass and redshift estimates.

5 CONCLUSIONS

In this paper we have analysed the outputs of a set of six cosmological simulations with the aim of describing the effect of massive neutrinos on the LSS of the Universe, focusing on the SZ and X-ray properties of galaxy clusters. Our simulations follow the evolution of a very large comoving volume, $2\,h^{-1}$ Gpc per side, allowing us to describe accurately the halo mass function up to masses above $10^{15}\ h^{-1}\,{\rm M}_\odot$, in two different cosmological scenarios, one adopting parameters consistent with the latest *Planck* results (Planck Collaboration XVI 2014) and another with the *WMAP* results (Hinshaw et al. 2013), both considering three different values of the sum of neutrino masses: $\Sigma\, m_\nu = (0, 0.17, 0.34)$ eV. The set of parameters used for these simulations is summarized in Table 1. Starting from the outputs of each simulation we constructed a set of 50 light cone

Downloaded from http://mnras.oxfordjournals.org/ at INAF Brera Milano (Osservatorio Astronomico di Brera) on January 9, 2015

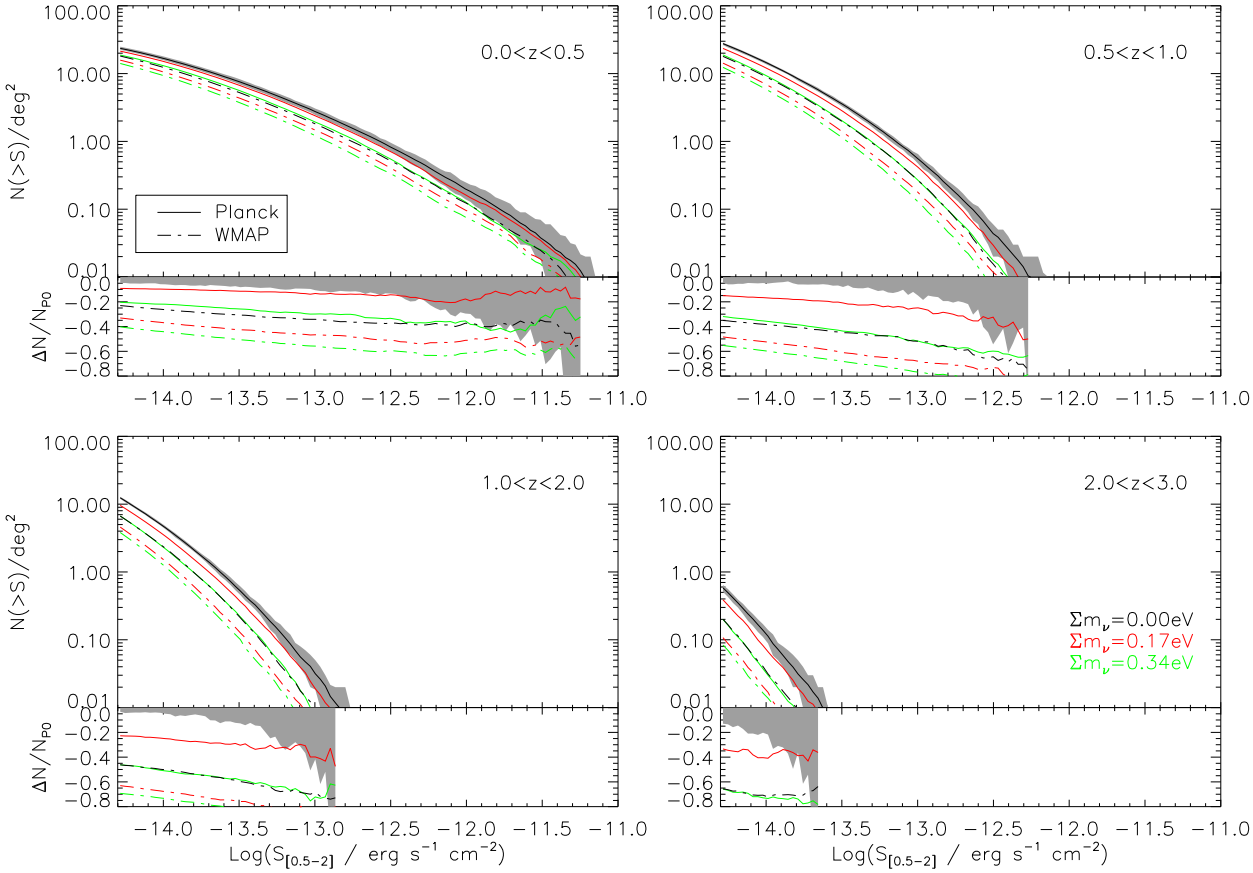

Figure 8. Same as Fig. 3, but for the number of galaxy clusters as a function of limit flux in the 0.5–2 keV band.

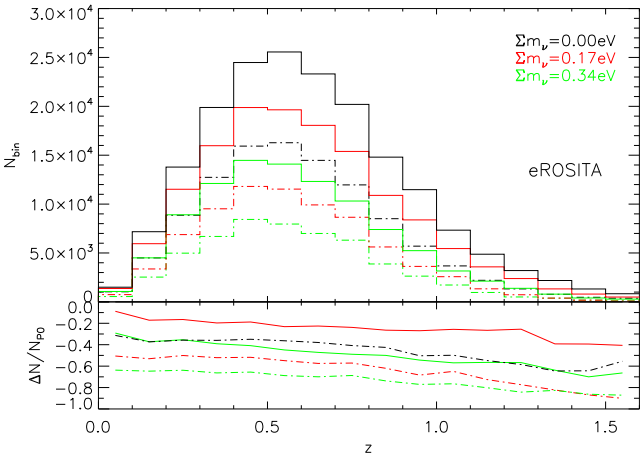

Figure 9. Predicted number counts in different redshift bins ($\Delta z = 0.1$) of galaxy clusters ($M_{500} > 10^{14}\,h^{-1}\,\mathrm{M}_\odot$) detectable by the *eROSITA* all-sky survey ($S_{[0.5-2]} > 3 \times 10^{-14}$ erg s^{-1} cm^{-2}) for our two sets of simulations. Lines and colour coding are the same as in Fig. 1. In the lower subpanel we show the fractional difference computed with respect to the P0 simulation.

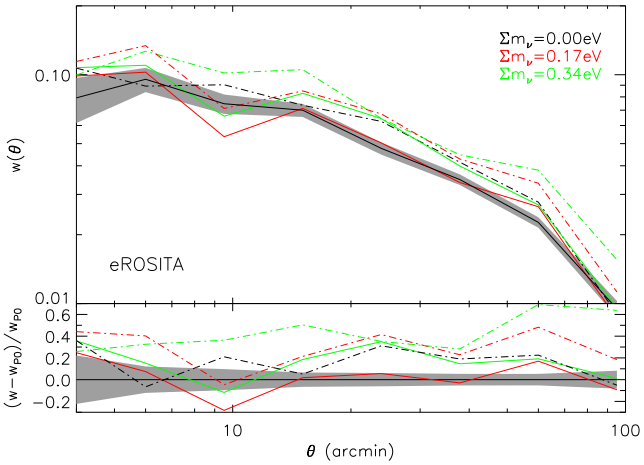

Figure 10. Correlation function as a function of the angular separation for the haloes detectable by the *eROSITA* cluster survey (see text for details). The grey-shaded area shows the Poissonian error (1σ) for the P0 simulation only computed over the 50 light cones (5000 deg^2). In the lower subpanel we show the fractional difference computed with respect to the P0 simulation.

catalogues of 10° per side and, by using known scaling relations, we computed the expected SZ and X-ray signals. This allowed us to test the effect of massive neutrinos on these observables, to compare them with *Planck* data and to investigate the capability of future cluster surveys of measuring $\Sigma\, m_\nu$ and disentangling its degeneracy with other cosmological parameters, mainly σ_8 and Ω_m. Our main results can be summarized as follows.

(i) As expected, the effect of massive neutrinos is larger at higher masses and redshift. At $z = 0$ neutrinos with masses $\Sigma\, m_\nu = 0.34$ eV decrease the number of haloes by 20–40 per cent in the mass range $M_{500} = 10^{13.5\text{–}14.5}\,h^{-1}\,\mathrm{M}_\odot$. While at $z = 0$ this is almost equivalent to a change in cosmology from the *Planck*–ΛCDMν model with $\Sigma\, m_\nu = 0.34$ eV to a simple *WMAP*–ΛCDM one, at higher redshift the effect of neutrinos is stronger.

Downloaded from http://mnras.oxfordjournals.org/ at INAF Brera Milano (Osservatorio Astronomico di Brera) on January 9, 2015

(ii) The spatial correlation function of the haloes is also influenced by $\Sigma\, m_\nu$ but with a smaller impact with respect to the mass function: about 15–20 per cent higher correlation for $\Sigma\, m_\nu = 0.34$, with lower dependence on scale and redshift. Conversely, the effect associated with a change in σ_8 and $\Omega_{\rm m}$ is larger and scale dependent, allowing for a possibility of breaking the degeneracy of $\Sigma\, m_\nu$ with these parameters.

(iii) The effect on the mass function translates into different expected counts of SZ detected clusters. Assuming a *Planck*–ΛCDM cosmology SPT will be able to detect about 1100 clusters, reduced by 40 per cent when $\Sigma\, m_\nu = 0.34$ eV. The same difference is found when computing the expected *Planck* detections in agreement with the findings of Planck Collaboration XX (2014). However this is marginally in tension with the suggested value of $\Sigma\, m_\nu$ =(0.20 ± 0.09) eV obtained when BAO constraints are included (Planck Collaboration XX 2014).

(iv) The global y-parameter value is strongly influenced by the presence of massive neutrinos. We observe an approximate scaling of $(1 - f_\nu)^{20}$ for the signal associated with galaxy clusters.

(v) While the shape of the SZ power spectrum shows a weak dependence on f_ν, its normalization scales as $(1 - f_\nu)^{25-30}$. The SPT and ACT results at $\ell = 3000$ are consistent with a *WMAP*–ΛCDM cosmology. If *Planck* cosmology is assumed instead, a value of $\Sigma\, m_\nu$ of about 0.34 eV is needed to fit with the data. We provide analytical fits to the power spectra (see equation 9 and Table 3).

(vi) Given the very high number of galaxy clusters above its flux detection limit, the *eROSITA* full-sky survey has the potential to put constraints on $\Sigma\, m_\nu$, provided that cluster redshifts will be measured. However model uncertainties and the degeneracy of $\Sigma\, m_\nu$ with both σ_8 and $\Omega_{\rm m}$ will make difficult to disentangle the two effects using its data alone.

Our work confirms how the LSS and galaxy clusters evolution are influenced by the value of the neutrino masses, the usefulness of cosmological analyses in measuring $\Sigma\, m_\nu$ and the necessity of extending the traditional ΛCDM concordance model to a more complete and accurate ΛCDMν cosmology. With the increasing number of upcoming surveys, statistical uncertainties will not constitute the main limitation in providing strong limits on the neutrino masses using galaxy clusters. On the other hand, degeneracies with other cosmological parameters and with the modelling (mainly scaling laws and redshift evolution) will require the combination of both CMB and LSS data coming from different observable quantities, allowing us to probe different epochs of structure formation. A list of possible new types of analyses that may provide constraints on neutrino mass includes redshift-space distortions, CMB weak lensing correlation and kinetic SZ power spectrum. We plan to investigate these further neutrino probes and their cross-correlations in the near future by exploiting the 'Dark Energy and Massive Neutrino Universe' (DEMNUni) simulation set (Carbone et al., in preparation; Castorina et al., in preparation), characterized by the same volume, but with a particle mass resolution about one order of magnitude larger than for the simulations adopted in the present work.

ACKNOWLEDGEMENTS

Most of the computations necessary for this work have been performed thanks to the Italian SuperComputing Resource Allocation (ISCRA) of the Consorzio Interuniversitario del Nord Est per il Calcolo Automatico (CINECA). MR and LM acknowledge financial contributions from contract ASI/INAF I/023/12/0, from PRIN MIUR 2010-2011 'The dark Universe and the cosmic evolution of baryons: from current surveys to Euclid' and from PRIN INAF 2012 'The Universe in the box: multiscale simulations of cosmic structure'. CC acknowledges financial support to the 'INAF Fellowships Programme 2010' and to the European Research Council through the Darklight Advanced Research Grant (#291521). We thank an anonymous referee that contributed to improve the precision of our results and the presentation of our work. We thank M. Brusa, S. Ettori, F. Marulli, F. Finelli, F. Petracca and M. Sereno for useful suggestions and discussions. We are particularly grateful to M. Viel for allowing us to access the non-public version of GADGET-3 modified to account for massive neutrino particles. We warmly thank A. Saro and J. Liu for providing us the data on the SPT noise.

REFERENCES

Ameglio S., Borgani S., Diaferio A., Dolag K., 2006, MNRAS, 369, 1459
Arnaud M., Pratt G. W., Piffaretti R., Böhringer H., Croston J. H., Pointecouteau E., 2010, A&A, 517, A92
Azzalini A., 1985, Scandinavian J. Stat., 12, 171
Battye R. A., Charnock T., Moss A., 2014, preprint (arXiv:1409.2769)
Beutler F. et al., 2014, MNRAS, 444, 3501
Bird S., Viel M., Haehnelt M. G., 2012, MNRAS, 420, 2551
Brusa M. et al., 2010, ApJ, 716, 348
Carbone C., 2013, Nucl. Phys. B Proc. Suppl., 237, 50
Carbone C., Verde L., Wang Y., Cimatti A., 2011, J. Cosmol. Astropart. Phys., 3, 30
Carbone C., Fedeli C., Moscardini L., Cimatti A., 2012, J. Cosmol. Astropart. Phys., 3, 23
Castorina E., Sefusatti E., Sheth R. K., Villaescusa-Navarro F., Viel M., 2014, J. Cosmol. Astropart. Phys., 2, 49
Cavaliere A., Fusco-Femiano R., 1978, A&A, 70, 677
Costanzi M., Villaescusa-Navarro F., Viel M., Xia J.-Q., Borgani S., Castorina E., Sefusatti E., 2013, J. Cosmol. Astropart. Phys., 12, 12
Costanzi M., Sartoris B., Viel M., Borgani S., 2014, J. Cosmol. Astropart. Phys., 10, 81
Costanzi Alunno Cerbolini M., Sartoris B., Xia J.-Q., Biviano A., Borgani S., Viel M., 2013, J. Cosmol. Astropart. Phys., 6, 20
Crawford T. M. et al., 2014, ApJ, 784, 143
Croft R. A. C., Hu W., Davé R., 1999, Phys. Rev. Lett., 83, 1092
Dolag K., Borgani S., Murante G., Springel V., 2009, MNRAS, 399, 497
Elgarøy Ø. et al., 2002, Phys. Rev. Lett., 89, 061301
Gonzalez-Garcia M., 2014, Phys. Dark Universe, 4, 1
Hasselfield M. et al., 2013, J. Cosmol. Astropart. Phys., 7, 8
Hinshaw G. et al., 2013, ApJS, 208, 19
Komatsu E. et al., 2009, ApJS, 180, 330
Komatsu E. et al., 2011, ApJS, 192, 18
Laureijs R. et al., 2011, preprint (arXiv:1110.3193)
Lesgourgues J., Pastor S., 2006, Phys. Rep., 429, 307
Lesgourgues J., Pastor S., 2012, preprint (arXiv:1212.6154)
Lesgourgues J., Pastor S., 2014, New J. Phys., 16, 065002
Lesgourgues J., Mangano G., Miele G., Pastor S., 2013, Neutrino Cosmology. Cambridge Univ. Press, Cambridge
Mak D. S. Y., Pierpaoli E., 2013, Phys. Rev. D, 87, 103518
Mantz A., Allen S. W., Ebeling H., Rapetti D., Drlica-Wagner A., 2010a, MNRAS, 406, 1773
Mantz A., Allen S. W., Rapetti D., 2010b, MNRAS, 406, 1805
Mantz A. B. et al., 2015, MNRAS, 446, 2205
Marulli F., Carbone C., Viel M., Moscardini L., Cimatti A., 2011, MNRAS, 418, 346
Merloni A. et al., 2012, preprint (arXiv:1209.3114)
Mohapatra R. N. et al., 2007, Rep. Progress Phys., 70, 1757
Planck Collaboration XVI, 2014, A&A, 571, A16
Planck Collaboration XX, 2014, A&A, 571, A20
Planck Collaboration XXI, 2014, A&A, 571, A21
Planck Collaboration XXIX, 2014, A&A, 571, A29
Predehl P. et al., 2007, Proc. SPIE, 6686, 668617

Downloaded from http://mnras.oxfordjournals.org/ at INAF Brera Milano (Osservatorio Astronomico di Brera) on January 9, 2015

Reichardt C. L. et al., 2012, ApJ, 755, 70
Reichardt C. L. et al., 2013, ApJ, 763, 127
Riemer-Sørensen S. et al., 2012, Phys. Rev. D, 85, 081101
Riemer-Sørensen S., Parkinson D., Davis T. M., 2014, Phys. Rev. D, 89, 103505
Roncarelli M., Moscardini L., Tozzi P., Borgani S., Cheng L. M., Diaferio A., Dolag K., Murante G., 2006a, MNRAS, 368, 74
Roncarelli M., Ettori S., Dolag K., Moscardini L., Borgani S., Murante G., 2006b, MNRAS, 373, 1339
Roncarelli M., Moscardini L., Borgani S., Dolag K., 2007, MNRAS, 378, 1259
Roncarelli M., Moscardini L., Branchini E., Dolag K., Grossi M., Iannuzzi F., Matarrese S., 2010, MNRAS, 402, 923
Roncarelli M., Cappelluti N., Borgani S., Branchini E., Moscardini L., 2012, MNRAS, 424, 1012
Rossi G., Palanque-Delabrouille N., Borde A., Viel M., Yèche C., Bolton J. S., Rich J., Le Goff J.-M., 2014, A&A, 567, A79
Rozo E. et al., 2010, ApJ, 708, 645
Sánchez A. G. et al., 2014, MNRAS, 440, 2692
Sereno M., Ettori S., Moscardini L., 2014, preprint (arXiv:1407.7869)
Shimon M., Rephaeli Y., Itzhaki N., Dvorkin I., Keating B. G., 2012, MNRAS, 427, 828
Sievers J. L. et al., 2013, J. Cosmol. Astropart. Phys., 10, 60
Spergel D. et al., 2013, preprint (arXiv:1305.5422)
Springel V., 2005, MNRAS, 364, 1105
Springel V., White S. D. M., Tormen G., Kauffmann G., 2001, MNRAS, 328, 726
Sunyaev R. A., Zeldovich Y. B., 1970, Ap&SS, 7, 3
Takeuchi Y., Kadota K., 2014, J. Cosmol. Astropart. Phys., 1, 46
Tegmark M. et al., 2006, Phys. Rev. D, 74, 123507
Thomas S. A., Abdalla F. B., Lahav O., 2010, Phys. Rev. Lett., 105, 031301
Viel M., Haehnelt M. G., Springel V., 2010, J. Cosmol. Astropart. Phys., 6, 15
Vikhlinin A. et al., 2009, ApJ, 692, 1060
Villaescusa-Navarro F., Bird S., Peña-Garay C., Viel M., 2013, J. Cosmol. Astropart. Phys., 3, 19
Villaescusa-Navarro F., Marulli F., Viel M., Branchini E., Castorina E., Sefusatti E., Saito S., 2014, J. Cosmol. Astropart. Phys., 3, 11
von der Linden A. et al., 2014, MNRAS, 443, 1973
Zhao G.-B. et al., 2013, MNRAS, 436, 2038

This paper has been typeset from a TEX/LATEX file prepared by the author.

Downloaded from http://mnras.oxfordjournals.org/ at INAF Brera Milano (Osservatorio Astronomico di Brera) on January 9, 2015